

# Waveguide Microwave Imaging: Spherical Inclusion in a Dielectric Sample

Alexander V. Brovko, Ethan K. Murphy, Matthias Rother, Heike P. Schuchmann, and Vadim V. Yakovlev, *Senior Member, IEEE*

**Abstract**—A new 3-D microwave imaging technique is proposed for the detection of a position and size of a spherical object in a dielectric sample located in a waveguide system. The reconstruction is based on a radial basis function neural network inversion, backed by finite difference time domain analysis and requires only elementary measurements of complex reflection and transmission coefficients. Functionality of the technique is illustrated by computational experiments in reconstructing the parameters of a glass sphere and an air bubble in a rectangular Teflon block. It is shown that, at 915 MHz, the spheres of not less than 15 mm diameter are reconstructed with the average errors of 0.9%–2.2%.

**Index Terms**—Finite difference time domain (FDTD) simulation, non-destructive evaluation (NDE), radial basis function (RBF) network, 3-D microwave imaging.

## I. INTRODUCTION

MICROWAVE imaging has recently emerged as a high-performance and cost-effective alternative to established techniques of non-destructive evaluation (NDE) and testing (NDT) [1]. The modern advances in the theory of and solution techniques for inverse problems in free space [2] has inspired substantial progress of microwave imaging in open systems (e.g., [3]–[5]) despite the fact that corresponding experimental implementations are typically quite complicated. While in terms of measurement, microwave imaging in closed systems may be simpler and provide high accuracy of measurements [6], it has not received an in-depth consideration so far—in part, possibly because of substantial complexity of theoretical aspects of the related inverse problems. However, there are applications for which microwave imaging in systems built on waveguides or resonators would be suitable and convenient; these include reconstruction of voids inside concrete

Manuscript received January 31, 2008; revised May 6, 2008. Current version published September 5, 2008. This work was supported by the EADS Company Foundation, German Academic Exchange Service (DAAD) and the Ministry of Education and Science of the Russian Federation.

A. V. Brovko is with the Department of Applied Information Technologies, Saratov State Technical University, Saratov 410070, Russia (e-mail: brovkoav@gmail.com).

E. K. Murphy was with Colorado State University, Fort Collins, CO 80521 USA. He is now with the Department of Mathematical Sciences, Worcester Polytechnic Institute, Worcester, MA 01609 USA (e-mail: ek-murphy@wpi.edu).

M. Rother and H. P. Schuchmann are with the Section of Food Process Engineering, Institute of Processes in Life Sciences, University of Karlsruhe (TH), Karlsruhe 76131, Germany (e-mail: matthias.rother@lvt.uni-karlsruhe.de; heike.schuchmann@lvt.uni-karlsruhe.de).

V. V. Yakovlev is with the Department of Mathematical Sciences, Worcester Polytechnic Institute, Worcester, MA 01609 USA (e-mail: vadim@wpi.edu).

Color versions of one or more of the figures in this paper are available online at <http://ieeexplore.ieee.org>.

Digital Object Identifier 10.1109/LMWC.2008.2002498

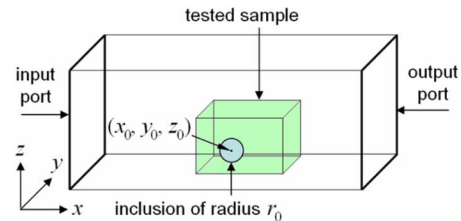


Fig. 1. Rectangular block with spherical inclusion in a waveguide system.

structures or bricks [7], detection of defects in wood slabs [8] and in composite panels [9], detection of porosity in ceramics and molded rubber [10] and monitoring of inhomogeneities in food products [11].

In this paper we present a new technique for the detection of a position and size of a spherical inclusion in a dielectric sample. In [3], [4], [12] a similar problem was solved for 2-D scenarios in free space; here, for the first time, our essentially 3-D technique is developed for a closed waveguide system. The proposed technique relies on an artificial neural network (ANN) used for inversion of the problem and reconstruction of parameters (i.e., a radius and spatial coordinates) of the sphere. A direct scattering problem is solved with the use of full-wave 3-D finite difference time domain (FDTD) analysis; corresponding numerical data are employed for network training and testing.

## II. METHOD

The structure under consideration consists of a single-mode rectangular waveguide containing a rectangular block (of known dielectric constant  $\epsilon'_1$ ) with a spherical inclusion (also of known dielectric constant  $\epsilon'_2$ ) as shown in Fig. 1. The goal is to find the 3-D position (i.e., the coordinates of the center,  $x_0, y_0, z_0$ ) and radius  $r_0$  of the inclusion. Reflection and transmission of the  $TE_{10}$  mode are measured in two (input and output) waveguide ports.

It has been found from the preliminary computations that  $S$ -parameters of this structure are particularly sensitive to the position of the inclusion along the direction of field propagation (the  $x$ -axis). This suggests that in order to retrieve information about the inclusion's position with respect to all three axes, one can deal with  $S$ -parameters corresponding to three sample's orientations ( $A, B, C$  in Fig. 2) rotated by  $90^\circ$  with respect to each other.

A radial basis function (RBF) network shown in Fig. 3 is used for reconstruction of parameters of the sphere. The ANN inputs are the real and imaginary parts of the reflection and transmission coefficients,  $S_{11}$  and  $S_{21}$  respectively, at the operating frequency  $f_0$  for three positions of the sample. The ANN outputs are the sought parameters of the sphere.

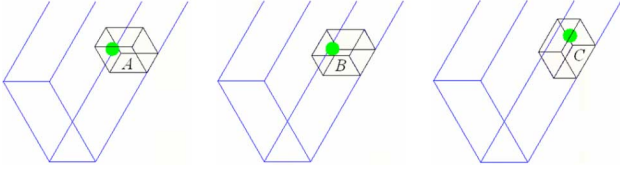


Fig. 2. Three orientation of the tested sample.

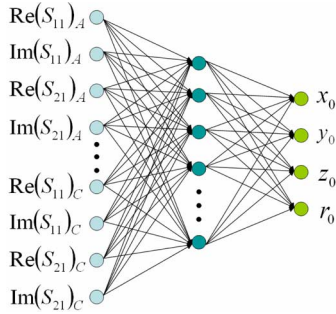


Fig. 3. Architecture of an RBF ANN.

The network with the global cubic RBF [13] is trained by numerical data obtained with the full-wave 3-D conformal FDTD simulator QuickWave-3D [14]. We generate pairs of input-output data such that the input sets are obtained for random combinations of  $x_0, y_0, z_0$  and  $r_0$  uniformly distributed in the specified domain. When the network is well trained, it is able to reconstruct the parameters of the inclusion from  $\text{Re}(S_{11})_A, \dots, \text{Im}(S_{21})_C$  measured in the corresponding experimental system.

The algorithm is implemented as a MATLAB code modifying the geometry of the structure, controlling operations of the FDTD simulator and processing its output.

### III. NUMERICAL RESULTS

In the computational experiments, we work with the WR975 ( $248 \times 124$  mm) waveguide section of 612 mm length. The tested rectangular ( $L_x \times L_y \times L_z = 100 \times 60 \times 80$  mm) block assumed to be made of Teflon ( $\epsilon'_1 = 2.06$ ) is shifted towards the waveguide wall to exclude symmetry.  $\text{Re}(S_{11})_A, \dots, \text{Im}(S_{21})_C$  are computed at  $f_0 = 915$  MHz. The sought parameters of the sphere are supposed to be in the following domain:  $5 \leq r_0 \leq 15$  mm,  $-34 \leq x_0 \leq 34$  mm,  $-14 \leq y_0 \leq 14$  mm,  $-24 \leq z_0 \leq 24$  mm, where the spatial coordinates are measured with respect to the center of the block.

In the first example, our algorithm is used to reconstruct parameters of a glass sphere ( $\epsilon'_2 = 6.0$ ). In Fig. 4, the network performance is illustrated for two reconstructed parameters. It is seen that the technique determines the parameters of a glass inclusion with a sufficiently high resolution—the network responses are very close to the testing points except for relatively small spheres. Naturally, the quality of microwave imaging depends on  $f_0$ ; here, with a guide wavelength of 437 mm, the accuracy of reconstruction deteriorates only for spheres of less than about 15 mm diameter.

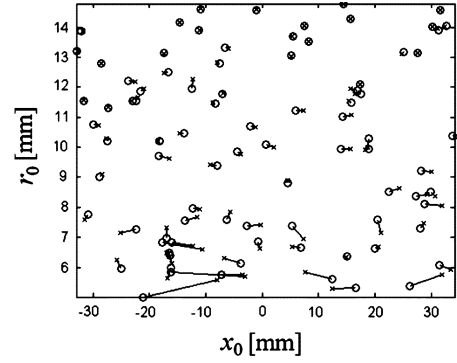
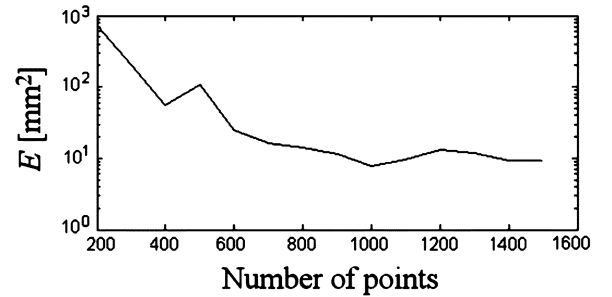
Fig. 4. Parameters  $x_0$  and  $r_0$  of the glass sphere found by the network ( $\times$ ) in response to 100 testing points ( $o$ ); numbers of training points is 1500.Fig. 5. Reconstruction of a glass sphere in the Teflon block: average error  $E$  versus the number of training points.

TABLE I  
RECONSTRUCTED PARAMETERS OF A GLASS SPHERE IN A TEFLON BLOCK

$S$	Position	$x_0$ , mm	$y_0$ , mm	$z_0$ , mm	$r_0$ , mm
1	Actual	-30	5	8	10
	Reconstructed	-29.5	4.3	7.1	10.1
	<b>error, %</b>	<b>0.5</b>	<b>1.1</b>	<b>1.1</b>	<b>1.3</b>
2	Actual	10	-5	20	11
	Reconstructed	11.8	-2.1	19.6	11.3
	<b>error, %</b>	<b>1.8</b>	<b>4.8</b>	<b>0.5</b>	<b>3.0</b>
3	Actual	7	3	-5	9
	Reconstructed	6.7	3.2	-4.6	9.1
	<b>error, %</b>	<b>0.3</b>	<b>0.3</b>	<b>0.6</b>	<b>1.2</b>
4	Actual	-32	-8	20	9
	Reconstructed	-32.9	-7.6	20.6	9.1
	<b>error, %</b>	<b>0.9</b>	<b>0.6</b>	<b>0.7</b>	<b>1.0</b>
<b>Ave. err. (12 sph.), %</b>		<b>1.4</b>	<b>1.8</b>	<b>0.9</b>	<b>1.0</b>

Quantitatively, we characterize the accuracy of the technique by the average total squared error constructed as

$$E = \frac{1}{100} \sum_{i=1}^{100} \left\{ \left[ x_{0a}^{(i)} - x_{0n}^{(i)} \right]^2 + \left[ y_{0a}^{(i)} - y_{0n}^{(i)} \right]^2 + \left[ z_{0a}^{(i)} - z_{0n}^{(i)} \right]^2 + \left[ r_{0a}^{(i)} - r_{0n}^{(i)} \right]^2 \right\}$$

where the squared differences are summarized for 100 randomly taken test points and the indices  $a$  and  $n$  denote the actual and network-reconstructed coordinates respectively. One can see from Fig. 5 that for the example with a glass sphere, the algorithm rapidly converges with the number of training points increasing up to 700–800; on the other hand, using more

TABLE II  
RECONSTRUCTED PARAMETERS OF AN AIR BUBBLE IN A TEFLON BLOCK

S	Position	$x_0$ , mm	$y_0$ , mm	$z_0$ , mm	$r_0$ , mm
1	actual	-30	5	8	10
	reconstructed	-31.2	4.2	8.6	10.1
	<i>error, %</i>	<i>1.2</i>	<i>1.3</i>	<i>-0.7</i>	<i>-1.4</i>
2	actual	10	-5	20	11
	reconstructed	9.4	-4.7	20.7	11.1
	<i>error, %</i>	<i>0.6</i>	<i>-0.5</i>	<i>-0.8</i>	<i>-0.5</i>
3	actual	7	3	-5	9
	reconstructed	8.2	3.8	-5.3	9.1
	<i>error, %</i>	<i>-1.2</i>	<i>-1.4</i>	<i>0.3</i>	<i>-0.9</i>
4	actual	-32	-8	20	9
	reconstructed	-33.3	-8.8	20.7	9.7
	<i>error, %</i>	<i>1.3</i>	<i>1.3</i>	<i>-0.9</i>	<i>-7.8</i>
<i>Ave. err. (12 sph.), %</i>		<i>2.2</i>	<i>1.0</i>	<i>1.4</i>	<i>1.8</i>

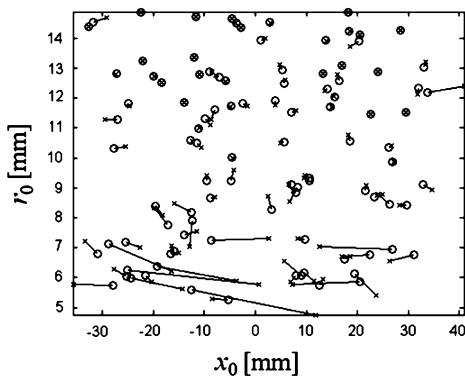


Fig. 6. Parameters  $x_0$  and  $r_0$  of the air sphere found by the network (x) in response to 100 testing points (o); numbers of training points is 750.

points may not result in substantial improvement of accuracy of reconstruction.

Table I numerically compares the reconstructed parameters of four glass spheres with their actual values. The maximal individual errors normalized to the block's or sphere's dimensions do not exceed 4.8% for the coordinates and 3% for the radius whereas the average errors computed for 12 tested spheres are not more than 1.8 and 1.0% respectively.

In the second example, the technique is used to reconstruct parameters of an air bubble ( $\epsilon'_2 = 1.0$ ). With half the number of training points than in the previous example, the network demonstrates a comparable performance for the air spheres of more than about 15 mm diameter (Fig. 6). While the maximal individual error of about 8% is observed in reconstruction of  $r_0$ , the average error in determining this parameter is still 1.8% (Table II).

It is worth noting that the presented accuracy of reconstruction is obtained for the low-contrast scenarios. In cases of high-contrast inclusions, the technique, due to the network generalization capabilities, may provide high quality of microwave imaging with smaller amounts of FDTD data sets.

Computational cost of the proposed technique is completely determined by the time spent on FDTD generation of data in comparison to which the time taken by the network operations is negligible. In the above examples, the data were obtained using a fine FDTD model of the entire system that contains nearly 80000 cells with the smallest ones of 4 mm. The steady state is reached roughly within 15000 time steps, and it takes 1 min

20 s of CPU time (Athlon 2.4 GHz processor PC). The computational cost could be reduced following the recommendations in [13]. Thus the algorithm can be used in a real-time microwave imaging system assuming that the FDTD computation is performed during the prior off-line phase of operation.

#### IV. CONCLUSION

A new 3-D microwave imaging technique, based on RBF ANN inversion and backed by FDTD analysis, has been proposed for locating and sizing a spherical inclusion in a dielectric sample. NDE is performed in a waveguide with the use of modeled and measured complex reflection and transmission coefficients for three spatial orientations of the sample. The computational experiments show that at 915 MHz the sizes and positions of glass and air spheres of more than 15 mm diameter in the  $100 \times 60 \times 80$  mm Teflon block are detected with the average error of 0.9%–2.2%.

The presented technique is directly applicable to the scenarios with lossy and metal inclusions and can be easily extended to cover the situations when dielectric constant of the inclusion is not known. In the latter case, it would be determined from the reconstruction performed with the network possessing one more output associated with  $\epsilon'_2$ . The method can also be straightforwardly adjusted to the inclusions of other (e.g., cylindrical, ellipsoidal, etc.) shapes.

#### REFERENCES

- [1] R. Zoughi, *Microwave Testing and Evaluation*. Amsterdam, The Netherlands: Kluwer, 2000.
- [2] D. Colton and R. Kress, *Inverse Acoustic and Electromagnetic Scattering Theory*. New York: Springer, 1998.
- [3] R. Mydur and K. A. Michalski, "A neural-network approach to the electromagnetic imaging of elliptic conducting cylinders," *Microw. Opt. Technol. Lett.*, vol. 28, no. 5, pp. 303–306, Mar. 5, 2001.
- [4] I. T. Rekanos, "On-line inverse scattering of conducting cylinders using radial basis-function neural networks," *Microw. Opt. Technol. Lett.*, vol. 28, no. 6, pp. 378–380, Mar. 2001.
- [5] A. Massa, M. Pastorino, A. Rosani, and M. Benedetti, "A microwave imaging method for NDE/NDT based on the SMW technique for the electromagnetic field prediction," *IEEE Trans. Instrum. Meas.*, vol. 55, no. 1, pp. 240–247, Feb. 2006.
- [6] T. Meyer, A. Jostingmeier, and A. S. Omar, "Microwave imaging using a novel regularization scheme," in *IEEE AP-S Int. Symp. Dig.*, Jun. 2003, vol. 3, pp. 175–178.
- [7] K. Belkebir, R. E. Kleinman, and C. Pichot, "Microwave imaging—Locations and shape reconstruction from multifrequency scattering data," *IEEE Trans. Microw. Theory Tech.*, vol. 45, no. 4, pp. 469–476, Apr. 1997.
- [8] M. Pastorino, A. Salvade, R. Monleone, T. Bartesaghi, G. Bozza, and A. Randazzo, "Detection of defects in wood slabs by using a microwave imaging technique," in *Proc. IEEE Instrum. Meas. Technol. Conf. (IMTC'07)*, Warsaw, Poland, May 2007, pp. 1–6.
- [9] N. Qaddoumi, G. Carrievau, S. Ganchev, and R. Zoughi, "Microwave imaging of thick composite panels with defects," *Mater. Eval.*, vol. 53, pp. 926–929, Aug. 1995.
- [10] A. J. Bahr, R. Zoughi, and N. Qaddoumi, "Microwave," in *Non-Destructive Evaluation. Theory, Techniques, and Applications*, P. J. Shull, Ed. New York: Marcel Dekker, 2002.
- [11] S. L. Taylor, *Advances in Food and Nutrition Research*. New York: Academic Press, 2006, vol. 51.
- [12] I. T. Rekanos, "Neural-network-based inverse-scattering technique for online microwave medical imaging," *IEEE Trans. Magn.*, vol. 38, no. 2, pp. 1061–1064, Mar. 2002.
- [13] E. K. Murphy and V. V. Yakovlev, "RBF network optimization of complex microwave systems represented by small FDTD modeling data sets," *IEEE Trans. Microw. Theory Tech.*, vol. 54, no. 7, pp. 3069–3083, Jul. 2006.
- [14] QWED, "QuickWave-3D, QWED," Warsaw, Poland, 2008 [Online]. Available: <http://www.qwed.com/pl/>